MEASUREMENT UNCERTAINTY OF A NEW MACHINE-INTEGRATED, PSD BASED APPROACH FOR THERMO-ELASTIC ERROR MEASUREMENT

CHRISTIAN BRECHER, ROBERT SPIERLING, MARCEL FEY

Laboratory for Machine Tools and Production Engineering (WZL), RWTH Aachen University, Germany

DOI: 10.17973/MMSJ.2022_06_2021191

corresponding author: R.Spierling@wzl.rwth-aachen.de

[Brecher 2021] presents a new, cost-efficient, machine-integrated measuring method for thermo-elastic errors of three-axis milling machines. The setup consists of a spindle mounted position-sensitive diode and a thermo-stable laser frame on the table. The initial paper contained a rough estimation of the measurement uncertainty and the uncertainty of the measureable errors.
This work presents a detailed analysis of the setup's measurement uncertainty in accordance with GUM 100. In addition the resulting uncertainties for the 13 measureable errors of the kinematic are updated based on the new results by means of a Monte Carlo simulation.

KEYWORDS

Machine tool, thermal error, measurement, measurement uncertainty, PSD

1 INTRODUCTION

The requirements for machine tools in terms of production quality, productivity and availability are constantly increasing. A major influence on quality issues is the thermo-elastic machine error which occurs when the structure of the machine tool is thermally affected by internal or external influences. This leads to a change in the thermal field of the machine structure, resulting in a deformation of the machine structure. This deformation of the machine structure ultimately causes a displacement of the tool center point (TCP) leading to machining errors on the produced parts. [Mayr 2012]

Research targets to reduce the thermo-elastic error to a minimum. In this context, highly accurate measurement methods are needed to determine the errors of the TCP in the machine volume. In addition, machine-integrated measurement setups enable an automated measurement during auxiliary time.

A new, cost-efficient, machine integrated optical measuring method for small and medium sized milling machines was developed. The setup consists of a spindle mounted position-sensitive diode (PSD) and a thermo-stable laser frame on the table. It is able to determine 13 of the 21 geometric errors in the machine volume. Thereby, the setup can fulfill industrial needs, such as cost-efficient measurement technology and high degree of automation of the measurement process by means of the machine integration. [Brecher 2021]

The existing work offers an estimation of the systems measurement uncertainty based on just a few quite uncertain asumptions. This paper targets to provide a more detailes analysis of the measurement uncertainty. In the following, state of the art (chapter 2), measurement setup and measurement procedure are described (chapter 3). Subsequently, a detailed measurement uncertainty calculation according to GUM100 is carried out (chapter 4). Consecutively, an updated Monte Carlo simulation derives the resulting uncertainties for the measurable thermo-elastic errors under consideration of the more detailed uncertainty (chapter 5). Finally, a summary of the procedure and an outlook on further possible research approaches are given (chapter 6).

2 STATE OF THE ART

There are various methods to determine thermo-elastic errors of machine tools. They can be classified in direct and indirect measurement methods. Indirect measurement methods derive deviations indirectly from the measured variables using kinematic models. Direct methods record individual deviations directly with a measuring device. The direct methods themselves can be divided into the three subcategories of calibrated normal-based methods, gravity-based methods and laser-based methods. The dominating laser based measurement devices are laser interferometers and a laser beam in combination with position sensitive diod (PSD). [Schwenke 2008]

This paper treats an approach categorized as a direct laser-based method, utilizing laser beam and PSD [Brecher 2021]. The laser beam provides a reference straight line in the machine volume by means of its beam propagation. PSD are large-area photodiodes that can quickly and accurately determine the position of an incoming light beam on the active surface of the diode. Therefore, they are well suited for metrological tasks around small geometric deviations. The impact of a light beam on the resistive coating on top of the PSD generates a photocurrent, which is discharged via the electrodes on the edge of the PSD. Assuming linearity, the position of the light spot can be derived from the partial currents. The area in which the assumption of linearity applies is limited to an area in the middle of the PSD. [Brecher 2021a] [Andersson 2008]

Two-dimensional PSD can be used for machine calibration, especially for the acquisition of straightness and resulting quantities such as squareness and parallelism. In [Schüßler 1971], basic measurements were carried out for the first time on the properties of lasers and PSDs when used in machine calibration. Measures to reduce the measurement uncertainties attributable to the laser source were presented in [Trapet 1982]. In [Rahneberg 2013], a PSD was integrated into a system for parallel acquisition of geometric errors in several degrees of freedom.

For two-dimensional PSD duolateral and tetralateral diodes are possible designs. They show different arrangement of electrodes, which results in different advantages and disadvantages, see Figure 1.

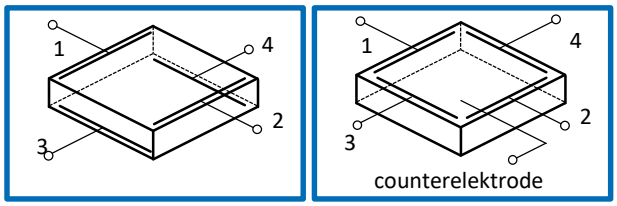

Figure 1 Two-dimensional PSD designs
duolateral (left); tetralateral (right) [Brecher 2021a]

Tetralateral diodes require calibration for better accuracy and show a lower liearity over the active surface . On the other hand, they are characterized by low dark current noise and higher

reaction speeds. In addition, they are less expensive. The duolateral diode is characterized by a low distortion in the edge region and a high resolution that can be achieved through a good signal-to-noise ratio. [Brecher 2021a] [Andersson 2008]

3 MEASUREMENT METHOD

This chapter summarizes the measurement setup and procedure presented in [Brecher 2021] as a basis for the measurement uncertainty evaluation in chapter 4. In addition a new basic verification measurement for the setup is presented.

3.1 Measurement setup

The measurement method is based on a laser source and two PSD. To enable squareness measurements, pentaprisms are added to the setup. For three-axis linear kinematics setup consists of a measurement head with duolateral PSD attached to the spindle and a thermo-stable, i. e. non-thermo-elastic-deforming, laser frame on the table. As the laser frame does not change its shape, variations of the acquired signals are considered to originate from the machine tool. Therefore, all measurements are compared to an initial reference measurement. In addition, this enables the use of low cost, less accurate components, e. g. pentaprisms, as the relative measurement cancels out the deviation of the laser beam from 90° comprised in both measurements.

Figure 2 (a) presents the laser frame consisting of carbon fibre rods with no overall thermo-elastic elongation. The rods are attached to pentaprism mounts and bearing points made of invar. Invar shows a very low thermo-elastic elongation of 1.7 µm/(m·K).

The measurement head is made of invar as well, see Figure 2 (b). Bandpass filters of 10 nm bandwidth protect the PSD from interfering light with bandwidth other than the laser beam (940 nm). The design is described in detail in [Brecher 2021].

The laser beam path is divided in five beam segments by the four pentaprisms redirecting the beam along the machine axes, see Figure 2 (c). The covered axis lengths in the workspace of the demonstrator machine is X 184 mm, Y 167 mm and Z 350 mm.

The main advantage of the setup is the low cost of the utilized parts and the machine integration enabeling an automated measurement.

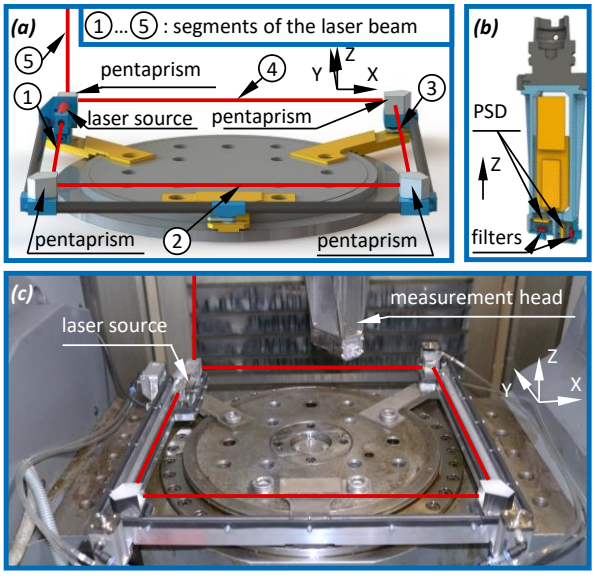

Figure 2. Laser beam and frame (a), measurement head (b), measurement setup including housing parts in a machine (c). [Brecher 2021]

3.2 Measurement procedure and strategy

A measurement is conducted by moving the spindle mounted measurement head (Figure 2(b)) to discrete measurement points in every segment. In accordance with [ISO 230-2] the segments comprise eleven measurement points with the exception of segment 1 comprising seven measurement points. In total there are 51 measurements points in all segments combined respectivily a full measurement run. The vertical PSD is placed perpendicular to the laser beam segments one to four by rotating the spindle. The horizontal PSD is used to measure segment five.

During the crossing of each segment, only a single feed axis is moved resulting in two measured straightnesses perpendicular to the feed directions. A unidirectional measurement of all segments takes four minutes. Reverse errors can be identified by performing a second measurement run with reversed feeds. This work focusses unidirectional measurements. The direction of movement is along the laser beam propagation.

To reduce the impact of noise on the results, the measured values of the PSD (sampling rate 100 Hz) are averaged for 150 values. The number of averaged values was derived as a compromise between measurement time of the whole procedure (4 minutes) and noise reduction.

Summarizing, this leads to ten measured straightnesses. A measurement model derives up to 13 measurable geometric machine tool errors. These errors comprise six straightnesses, three squarenesses, two positioning accuracies (X- and Y-axis) and two roll errors of the three axes kinematic. A more detailed explanation, how the 13 errors are calculated is given in [Brecher 2021].

3.3 Basic verification measurement

For the new measurement method a first validation utilizing the measurement systems of the machine tool has been presented in [Brecher 2021]. Nevertheless, a more detailed validation utilizing a commercial measurement device is necessary.

The basis for all further error calulation are the straighness measurements in the five segments in two dimensions each. For validation purposes a validation measurement with an industry standard measurement device Renishaw XM-60 is performed. The measurement uncertainty of the device amounts 1.5 µm (95%, k=2). The measurement setup is displayed for Segment 2 in figure 3. The measurement head and the commercial measurement system are next to eachother both attached to the machine spindle (not shown in the figure).

The measurement procedure of the new method utilizing an initial reference measurement is simulated. Therefore, such initial reference measurement is performed along an NC path. For the second measurment the NC path is manipulated and both devices measure again. The difference of both measurements is then compared. Please note, that this measurement is performed under real workshop conditions inside a meachine tool. Consequently, the results are pertubated by the thermo-elastic error of the machine tool between the different meausrements attributing to one measured difference. Both measurements can be conducted in less than 10 minutes reducing such perturbation.

All segments have been measured, see figure 4. In addition the root mean square error (RMSE) of the measured differences is given. It can be seen for all three repeated measurements, that all results of the new setup are inside the measurement uncertainty range of the commercial system (here 3 µm (95%, k=2) as a difference of two measurements is shown).

The three measured differences of each segment can not be considered for a measurement uncertainty calculation in accordance with GUM 100 Type A, as the thermo-elastic error of the machine tool inbetween the six base measurements (two per measured difference) would be attributed as well [JCGM 2008a]. For such calculation the measurements must be repeated on a machine tool that has a powerful temperature control system for machine-internal causes of thermo-ealstic errors (e. g cooling systems for structural components), to minimize such influecen.

Summarizing, for all measurements the uncrtainty range of the industrilal device is met. So for all five segments a validation by means of an industrial measurement device is given.

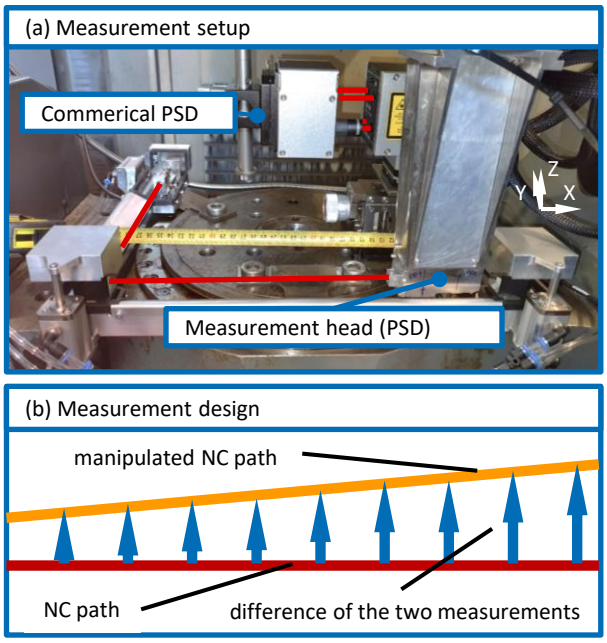

Figure 3. Measurememnt setup (a) and measurement design (b)

4 PSD MEASUREMENT UNCERTAINTY ANALYSIS

This chapter presents an evaluation in accordance with GUM 100. The utilized fundamentals of the standard are presented in (4.1). As stated in chapter 3, an overall evaluation in accordance with GUM 100 Type A is not promissing. Therefore, the relevant influences are identified (4.2). The next step quantifies the impact of the identified influences (4.3). The summation of the overall PSD uncertainty concludes chapter (4.4).

4.1 Fundamentals of GUM 100

The GUM100 guideline offers two procedures to determine an uncertainty. In the determination according to type A, an uncertainty u is determined via repeated measurements from the standard deviation σ of the measured values q_k and the number of measurements n, see eq. (1).

$$u = \frac{\sigma(q_k)}{\sqrt{n}} \tag{1}$$

In the determination according to type B, the uncertainties are calculated from probability density distributions which can be derived from other sources of information, e.g. data sheets. For the case of a normal distribution, the uncertainty u_{normal} corresponds to the standard deviation σ of the mean value, see eq. (2). In the case of a rectangular distribution, the uncertainty $u_{rectangular}$ is calculated using eq. (3), where Δa represents the distance of the interval boundaries from the mean value.

$$u_{normal} = \sigma \tag{2}$$

$$u_{rectangular} = \frac{\Delta a}{\sqrt{3}} \tag{3}$$

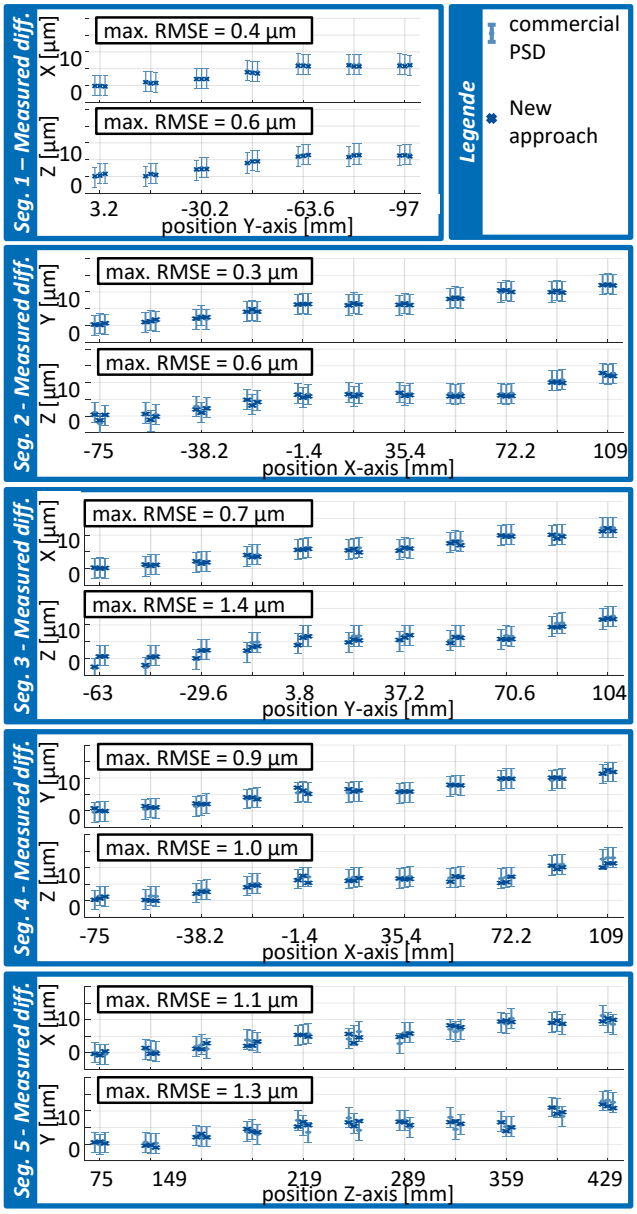

Figure 4. Measurement results

The calculation of combined uncertainties u_c follows eq. (4). For the case of uncorrelated random variables in this work, the gradients of the standard uncertainties c_i equal 1. u_i represents the individual uncertainties.

$$u_c = \sqrt{\sum_{i=1}^{n} (c_i \cdot u_i)^2} \tag{4}$$

4.2 Identification of relevant influences

To determine the relevant influences, Pfeifer's Method of the 5M is applied [Pfeifer 2010]. It categorizes the influences into measurement operator, measurement object, measurement method, measurement environment and measurement device. The relevant influences are shown in Figure 5. For the presented automated method an influence of the measurement operator

does not exist. Nor is there an impact of the measurement method.

The thermo-elastic behavior of the machine tool, respectively the measurement object, could affect the measurement uncertainty during the measurement. The quantification necessitates a model of such behavior. The model requires measurements of the thermo-elastic behavior, that can be delivered by the presented measurement method. Therefore, a quantification in advance is not possible and would always be machine tool specific. Consequently, this possible influence is neglected in this work.

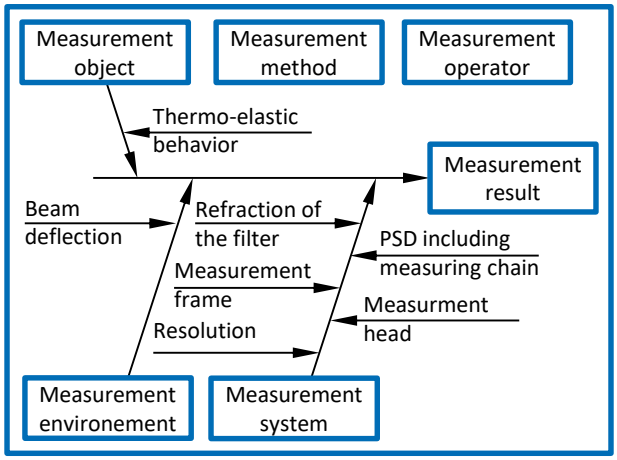

Figure 5. Relevant influences

4.3 Quantification of the influences

Measurement head

A thermo-elastic elongation of the measurement head in Z-direction affects the PSD measurement in the segments 1 to 4 in this direction. The error in the Z-direction is linearly corrected, see eq. (5). The thermal elongation Δl_{th} is calculated from the initial length l_0, the coefficient of thermal elongation α_{th} and the temperature change ΔT.

$$\Delta l_{th} = l_0 \cdot \alpha_{th} \cdot \Delta T \tag{5}$$

In the following, the uncertainty of the correction is quantified. All determined uncertainties are based on the assumption of a rectangular distribution and can thus be calculated using eq. (3) and eq. (5).

ΔT of the measurement head is acquired with a PT100 temperature sensor on the inside of the structural part. A measurement of the variation of ΔT over seven days showed ±0.85 K of temperature change, see figure 6. The maximum variation is estimated with ±2 K to the safe side for this work.

The measurement head made of invar shows a thermal elongation of α_{th} = 1.7 µm/(m·K). According to **[BRYAN 1968]** the uncertainty of such coefficients amounts up to ±25%, resulting in ±0.43 µm/(m·K).

The initial length l_0 of the measurement head amounts 193 mm and is estimated for the milled part with an potential error of 0.1 mm respectively ±0.05 mm.

This results in an uncertainty $u_{initial\ length}$ = $1 \cdot 10^{-4}$ µm which is considered to be negligible. The uncertainty resulting from the thermo elongation coefficient is $u_{\alpha th}$ = 0.10 µm.

The error of the temperature measurement consists of the error of the utilized PT100 sensor of ±0.25 K (class A according to IEC 751-DIN EN 60751; for a measurement range of ±50°C) and the error of the temperature measurement chain of ±0.1 K (for the measurement range of 0 to +60°C). This results in the uncertainties u_{sensor} = 0.05 µm and u_{chain} = 0.02 µm.

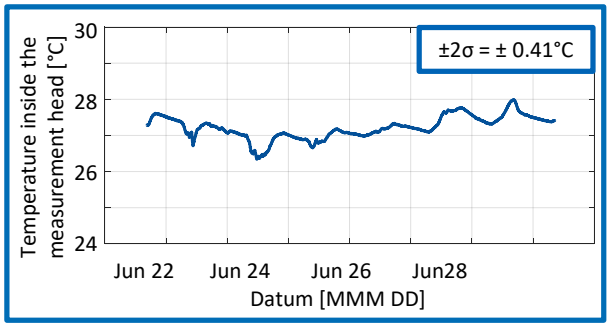

Figure 6. Temperature variation inside the measurement head

The measurement head is attached to the machine spindle with a HSK-T 63 tool interface. The tool change repeatability of the interface results in errors of the measured values. According to **[Wagner 2017]** there are better results for a changing process, if the tool interface is manually rotated against the tappet pieces inside the spindle. For the research work this is done manually. In case of an industrial use, a spring preloaded adaptor at the tool interface might be suitable. The relevant standard uncertainties are listed in table 1.

repeatability	standard deviation	sample size
axial	0.27 µm	25
radial	0.21 µm	27
rotational	0.10 µm/m	7
rotational for max. PSD lever 26,2 mm	0.26 µm	7

Table 1. Repeatability of the tool interface for a tool change

Under use of eq. (1) these standard deviations result in u_{ax} = 0.05 µm, u_{rad} = 0.04 µm and u_{rot} = 0.10 µm. To simplify the overall balance, the axial and radial influence are estimated with $u_{measuring\ head}$ = 0.10 µm to the safe side.

Measurement frame

The measurement frame introduced in chapter 3.1 consists of pentaprisms made of glass, that are mounted on invar carriers. A linear elongation of the pentaprisms has no effect on its function. The carriers are connected with carbon fiber rods with titanium end pieces, see figure 7.

The rods show no thermo-elastic elongation due to a winding tuned to the thermo-elastic elongation of the titanium end pieces. The carriers show a thermal elongation of 1.7 µm/(m·K)±0.43 µm/(m·K), as discussed above. The distance of the rod's mounting surface to the mounting point of the pentaprism amounts 18 mm (X- and Y-direction) and 5 mm (Z-direction), see figure 7.

In X-direction there is an additional invar piece of 30 mm length serving as a mounting point for the frame. Together with the two carriers the resulting temperature related thermo-elastic elongation in X-direction for the mounting point and two carriers amounts to 0.12 µm/K. The temperature variation measured inside the measurement head is considered to be a good estimation for the inner temperature variation of the invar parts. The measured temperature variation is 1.7 K, see figure 6. The resulting uncertainty is calculated under the assumption of a rectangular distribution to u_{frame} = 0.12 µm using eq. (3) and eq. (5), as described in the last section. To reduce the complexity of the uncertainty estimation, this value is used for all coordinate directions.

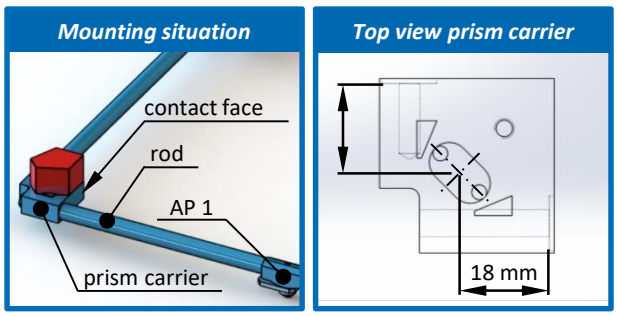

Figure 7. Assembly of the measurement frame

PSD resolution

The resolution of the PSD measurement is 0.1 µm. The signal processing with the moving average filter enables a higher resolution. The difference of neighbouring values is smaller than ±0.1 µm, see figure 8. The final measurement values are chosen from the middle of the standstill interval of the measurement. Nonetheless, the effect is taken into account with ±0.1 µm as an estimation to the safe side which leads to an uncertainty $u_{resolution}$ = 0.06 µm using eq. (3).

Beam deflection

The wavelength of light passing through a medium is dependent on the refraction index of the medium. The refraction index of air is influenced by the gradients of air-temperature, -pressure and humidity as well as its chemical composition. The chemical composition can be neglected for most production engineering applications [Jatzkowski 2011]. The air temperature has the largest impact.

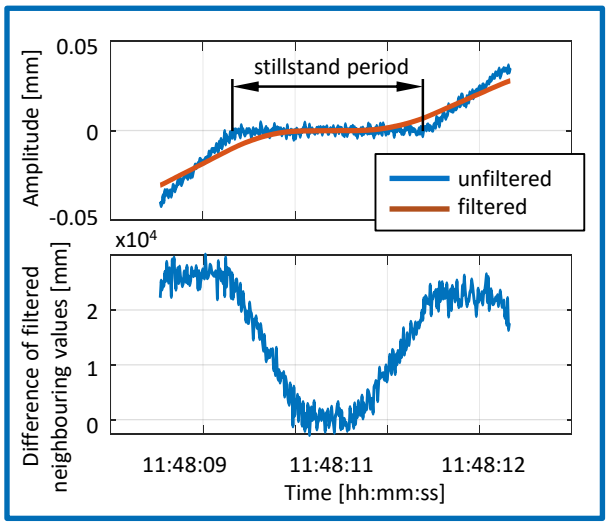

Figure 8. Resolution of the averaged values

[Jatzkowski 2011] calculated that for a temperature gradient of 0.7°C/m over a distance of 1.5 m the maximum laser beam deflection perpendicular $y_{0.7}$ to the direction of the beam propagation x amounts 0.75 µm. This factor needs to be considered dependent on the distance of a measurement point to the beam source, see eq. (6).

$$y_{0.7} = 1/3 \cdot x^2 \tag{6}$$

As the beam path borders a volume (approx. 350 mm x 320 mm x 400 mm), the gradient would result in a lower variation along the beam path. To the authors opinion the chosen gradient is an estimation to the safe side allowing to neglect the other gradients due to their lower impact.

In order to prevent turbulence, which is not taken into account in this consideration, the use of the measuring system is restricted to machines with an enclosed working space. If the sealing air is switched off for the measuring process and there is no draught from outside, the author assumes that possible interference is greatly minimized.

Refraction of the filter

While passing through the filter, which is shielding the PSDs from interfering light from the environment, the laser beam is deflected if the beam is not perpendicular to the filter surface. The geometric situation is shown in figure 9.

The initial cross set of the laser beam s_0 is calculated by eq. (7). The inclination angle α and the width of the filter have to be known. The deflection in the filter s_B made of glass is calculated by eq. (8), utilizing the refraction index of the filter material β. The axial deflection Δs on the PSD is calculated by the difference of the two values, see eq. (9). Due to the measurement principle of comparing a measurement with a reference measurement, only the change of the gradient angle α is of relevance, as the refraction inside the filter is constant. Thereby the gradient of the deflection ∇s is calculated, see eq. (10).

$$s_0 = d \cdot tan(\alpha) \tag{7}$$

$$s_B = d \cdot tan(\beta) \tag{8}$$

$$\Delta s = d \cdot ta\,n(\alpha) - d \cdot tan(\beta) \tag{9}$$

$$\nabla s = d \cdot (tan(\alpha + \dot{\alpha}) - tan(\alpha)) \tag{10}$$

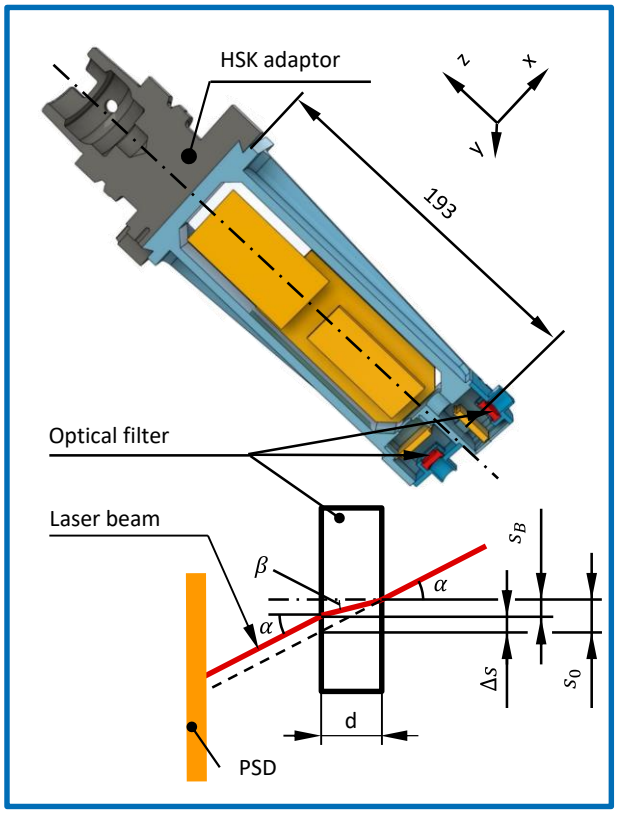

Figure 9. Geometrical situation of PSD and filter

The authors estimate a possible angular error $\dot{\alpha}$ of the machine tool of the named size to 100 µrad to the safe side. An additional distortion originating from the tool interface could amount 10 µrad, see table 1. As the gradient of the tangent function used in eq. (10) rises along the interval from 0 to 2π, the estimation of the initial angle α is performed to the safe side by choosing the maximum measurable angle of the system. The PSD length amounts 10 mm and the longest laser beam segment has a length of 400 mm. Consequently, the maximum possible angle

amounts 25 mrad. With a filter width d of 5 mm the maximum beam deflection amounts to ±0.55 µm. For the assumption of a rectangular distribution this leads to an uncertainty $u_{refraction}$ = 0.32 µm.

PSD including measuring chain

The error of the PSD is determined by means of calibration. The original measuring chain and signal processing (see 3.2) are utilized as well. The measurement head (not displayed), including the PSD, is placed on the table of a 3-axis high precision kinematic, see figure 10.

The PSD axes are aligned with the axis of the kinematic. The laser source moves stepwise along a tight grid of measurement points. The shift of the laser source is measured in two dimensions with the help of a laser based high precision CCD displacement sensor. The PSD error is derived from the difference of the PSD and the CCD measurement, see figure 11. The calibrated error is corrected for all future PSD measurements. The values between two grid points are interpolated over the interpolation distance of 0.1 mm.

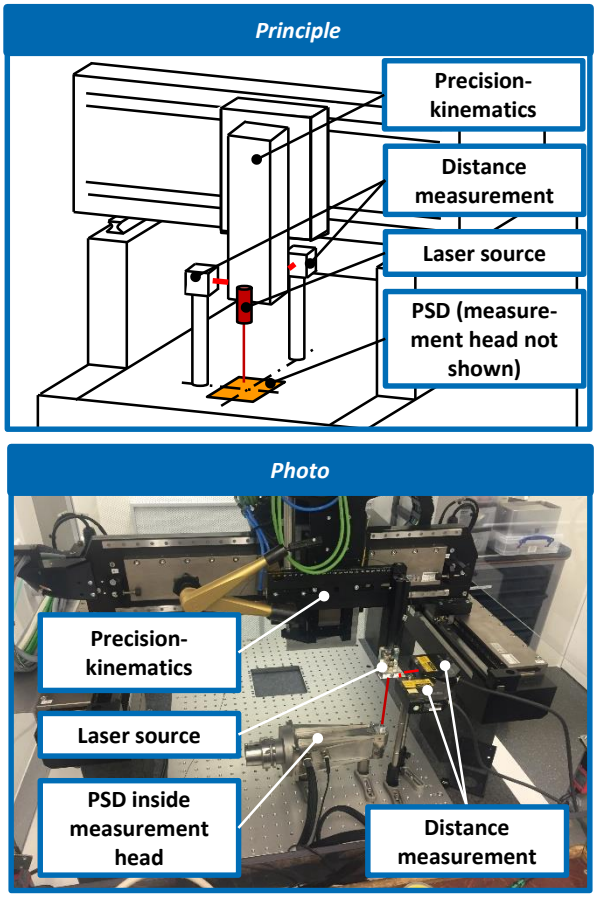

Figure 10. Setup of the PSD error measurement

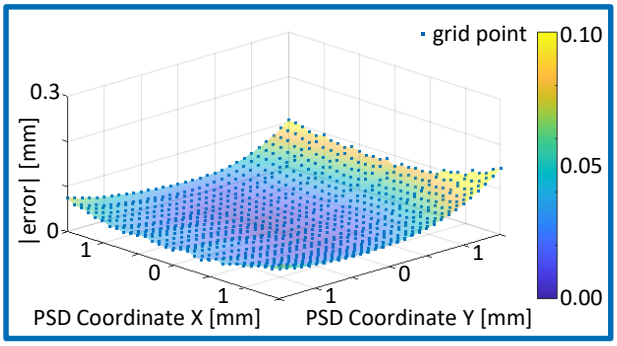

Figure 11. Error of the PSD in Segment 5 (see Fig. 1)

The uncertainty of the determined values corresponds to the uncertainty of the laser-based displacement measurement. This consists of a linearity deviation of ±0.05% of the measuring range and a repeatability of 0.05 µm. By limiting the measuring range for the individual segments according to table 2, the stated uncertainties are calculated according to eq. (4) respectively eq. (11). The summation is based on the assumption of a linear model of the measurement without interaction between the individual contributions. For the uncertainties related to the measurement point it must be taken into account, that the laser beam in the individual segments is skewed in space. This propagates through the frame and leads to larger maximum related uncertainties in the segments grow with the beam length. However, the measurement paths of all segments are aligned symmetrically within the measurement range of the PSD. The PSD therefore records significantly smaller values in the middle of the segments causing smaller uncertainty contributions for these measurement points. These uncertainties are taken into account for the individual measurement positions.

$$u_{PSD} = \sqrt{\left(1 \cdot \frac{lin.deviation/2}{\sqrt{3}}\right)^2 + (1 \cdot 0.05\mu m)^2} \qquad (11)$$

PSDs can be subject to temperature-dependent fluctuations. However, the installation situation of the PSD in the measuring head ensures very low temperature fluctuations, see figure 6. A maximum temperature fluctuation of 1.7°C occurred during a random test of 7 days. The dependence of the PSD values on the temperature will not be considered further below, due to the low temperature fluctuation in the measuring head.

Segment	Measure-ment range PSD [mm]	Linearity deviation [µm]	max. u_{PSD} [µm]
1	X ±0.20 Z ±0.30	X 0.4 Z 0.6	0.13 0.18
2	Y ±0.20 Z ±0.60	Y 0.4 Z 1.2	0.13 0.35
3	X ±0.20 Z ±0.30	X 0.4 Z 0.6	0.13 0.18
4	Y ±0.25 Z ±0.35	Y 0.5 Z 0.7	0.15 0.21
5	X ±1.3 Y ±0.6	X 2.6 Y 1.2	0.75 0.35

Table 2. Parameters of the PSD uncertainty

4.4 Summation of the influences

Finally, the relevant influences quantified in chap. 4.2 (see tab. 3) are summed up in accordance with eq. (4). The resulting maximum combined standard uncertainty u_c amounts 1.13 µm.

Finally, the confidence interval is determined by multiplying the combined standard uncertainty by the coverage factor k, see eq. (11). For this work an interval of confidence of 95% respectively k = 2 is applied.

$$U_{max} = k \cdot u_{c\,max} \qquad (11)$$

This leads to the maximum expanded uncertainty of the measurement procedure U_{max} = 2.26 µm (interval of confidence = 95%).

Individual uncertainty	u_i [µm]	c_i
Beam refraction inside the optical filter	0.32	1
Resolution	0.06	1
Measuring-frame	0.12	1
Measuring-head: co-efficient of thermal expansion	0.10	1
Measurement-head: temperature sensor	0.05	1
Measurement-head: temperature measuring chain	0.02	1
Tool interface	0.10	1
Deflection of the laser beam	position dependent max. 0.75	1
PSD including measure-ment chain	Position dependent max. 0.75	1

Table 3. Summary of the individual uncertainties and their gradients

5 MONTE CARLO SIMULATION OF THE GEOMETRIC ERRORS

A Monte Carlo simulation is a suitable method to determine the uncertainties of the used model [JCGM 2008a] [JCGM 2008b] [WILHELM 2001]. In the context of this work, the uncertainties of the individual errors of the measurement model are determined. The procedure is shown in Figure 12.

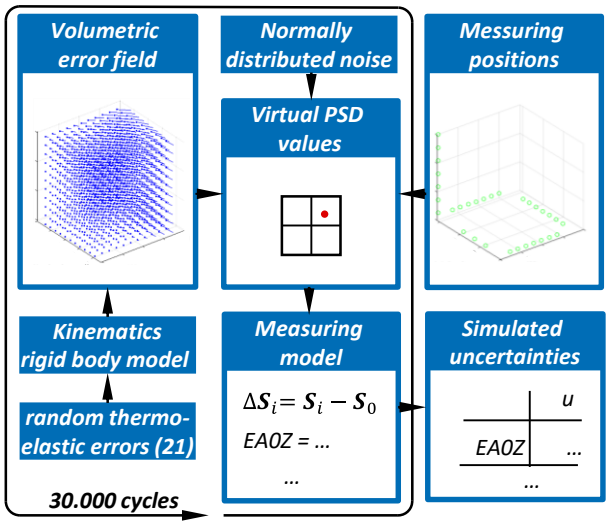

Figure 12. Applied procedure of the Monte Carlo method

An initial Monte Carlo simulation has been published in [Brecher 2021]. Here the results are updatet. The update takes into account the more accurate measurement uncertainty of the last chapter.

Initially, 21 thermo-elastic errors of the linear three-axis kinematics of the demonstrator machine are generated randomly, following [BRINGMANN 2007]. The amplitudes of the individual errors are estimated on the basis of [WENNEMER 2018] to the safe side. In addition, they are multiplied by the safety factor 3 in order to also account for larger deviations.

These random thermo-elastic errors are fed into a rigid body model of the kinematics according to Denavit Hardenberg [DENAVIT 1955]. The kinematics is a [wbXYZt] kinematics according to ISO 10791-6 [ISO 2014]. The result of this calculation is a volumetric error field in the working space.

In the next step, virtual measured values are determined at eleven points per segment analogous to the procedure of the real measurement (see chap. 3.1). Normally distributed noise of the PSD u_{sum} is added to the virtual measured values according to the analysis of the measurement uncertainty in chapter 3.2. To take the influence of the subtraction of a reference measurement into account, the noise is doubled additionally.

Subsequently, the measurement model according to [Brecher 2021] is used to derive the thermo-elastic errors. For the described procedure, 30000 simulation cycles are carried out. The uncertainties U (k=2, 95%)are determined from the results of the simulation runs, see Tab. 4.

Error	U [µm]	Error	U [µm]	Error	U [µm]
EYX	±1.3	EZY	±3.9	EAX	±8.2 *
EZX	±1.6	EYZ	±3.4	EBY	±6.4*
EXY	±1.5	EXX	±0.4	EA0Z	±4.2*
EXZ	±1.5	EYY	±0.4	EB0Z	±4.9*
*max. resulting linear uncertainty with respect to the measurement volume				EC0Y	±4.4*

Table 4. Updated resulting uncertainties from Monte Carlo Simulations

6 CONCLUSION AND OUTLOOK

This apper presents a more advanced validation measurement for the PSD based new method. Utilizing an industrial measurment device. For all measurements the uncrtainty range of the industrilal device is met. So for all five segments of the new setup a validation by means of an industrial measurement device is given.

A more detailed uncertainty analysis for the measurement method of [Brecher 2021] was presented as well. The extended measurement uncertainty of the measurement setup and the resulting uncertainties for the measureable thermo-elastic errors were outlined. Based on a systematic assessment of the relevant effects nine contributing influences have been quantified using the GUM 100 method. Based on the new results the existing monte carlo simulation of the measureable machine errors uncertainty has been updated.

A useful next step would be a measurement validation of the combined standard uncertainty would be useful. But for doing this under workshop conditions a machine tool with a controlled thermo-elastic errors is necessary, as these errors perturbate the measurement.

For further improvements of the measurement uncertainty the use of super-invar is a possible approach. In addition, a more detailed analysis of the laser beam deviation due to gradients of the air temperature, pressure or humidity seems promising and can contribute to the topic in a valuable way.

ACKNOWLEDGMENTS

The presented findings are funded by the Deutsche Forschungsgemeinschaft (DFG, German Research Foundation) – 419982228.

REFERENCES

[Andersson 2008] Andersson, H. Position sensitive deterctors – Device technology and applications in spectroscopy. Sundsvall: Department of information technology and media, Mid Sweden University, 2008

[Brecher 2021] Christian Brecher, C., Spierling, R., Fey, M. and Neus, S. Direct measurement of thermo-elastic errors of a machine tool. CIRP Annals, 2021, Vol.70, No.1, pages 333-336, ISSN: 0007-8506

[Brecher 2021a] Brecher, C., Weck, M. Machine Tools Production Systems 2 – Design, Calculation and Metrological Assessment. Berlin: Springer Verlag GmbH, 2021

[BRINGMANN 2007] Bringmann, B. Improving geometric calibration methods for multi-axis machining centers by examining error interdependencies effects. Zurich: ETH Zurich, 2007

[Bryan 1968] Bryan, J. International Status of Thermal Error Research. CIRP Annals, 1968, pages 203-215

[DENAVIT 1955] Denavit, J., Hartenberg, R. S. A kinematic notation for lower-pair mechanisms based on matrices. Applied Mechanics, 1955, Vol.22, pp 215–221

[ISO 2014] 10791-6 (2014-12-00). Test conditions for machining centres.

[ISO 230-2] Test Code for Machine Tools - Part 2. Determination of Accuracy and Repeatability of Positioning of Numerically Controlled Axes, ISO, Geneva.

[Jatzkowski 2011] Jatzkowski, P. Resource-efficient calibration of 5-axis machine tools with tracking interferometers (in german). ISBN 3863590112. RWTH Aachen University, 2011.

[JCGM 2008a] Guideline JCGM 100:2008. Evaluation of measurement data. Guide to the expression of uncertainty in measurement. September 2008

[JCGM 2008b] Guideline JCGM 100:2008. Evaluation of measurement data. Supplement 1 to the "Guide to the expression of uncertainty in measurement" – Propagation of distributions using a Monte Carlo method. 2008

[Mayr 2012] Mayr, J. et al. Thermal issues in machine tools. CIRP Annals, 2008, Vol.61, Issue 2, p. 771-791, ISSN 0007-8506

[Noll93] Noll, R., Donges, A. Laser measurement technology – basics and application, vol. 4 (in german). Heidelberg: Hüthig Buch Verlag, 2006

[Pfeifer 2010] Pfeifer, T. and Schmitt, R. Fertigungsmesstechnik. Oldenbourg: Wissenschaftverlag, 2010. ISBN 3486592025

[Rahneberg 2013] Rahneberg, I. Investigation of optical multi-component measuring systems (in german). Illmenau, 2013

[Renishaw 2017] Renishaw PLC. Renishaw introduces the new XM-60 6D laser system (in german). Wotton-under-edge, 2017

[Schüßler 1971] Schüßler, H.-H. The suitability of laser beams and photoelectric detectors for measuring the deviation of straightness and flatness in mechanical engineering (in german). Aachen: RWTH Aachen university, 1971

[Schwenke 2008] Schwenke, H. et. al. Geometric error measurement and compensation of machines – an update. CIRP Annals, 2008, Vol.57, No.2, pp 660-675

[Trapet 1982] Trapet, E. A contribution to the reduction of the measurement uncertainty of laser-based alignment measurement systems (in german). Aachen, RWTH Aachen university, 1982

[Wagner 2017] Wagner, P. Tool interfaces for lathes (in german). ISBN 3863595678. RWHT Aachen University, 2017.

[Wennemer 2018] Wennemer, M. Method for the metrological analysis and characterization of volumetric thermo-elastic displacements of machine tools (in german). Aachen: Apprimus Verlag, 2018

[Wilhelm 2001] Wilhelm, R. G.; Hocken, R.; Schwenke, H.: Task specific uncertainty in coordinate measurement. CIRP Annals, 2001, Vol.50, No.2, pp 553–563

CONTACTS:

Robert Spierling, M. Sc.
Laboratory for Machine Tools and Production Engineering (WZL) of RWTH Aachen University
Campus-Boulevard 30, 52074 Aachen, Germany
+49 241 80 24781, r.spierling@wzl.rwth-aachen.de, https://www.wzl.rwth-aachen.de